International Geology Review, Vol. 48, 2006, p. 1113–1132.

Role of Crustal Contamination in Formation of the Jinchuan Intrusion and Its World-Class Ni-Cu-(PGE) Sulfide Deposit, Northwest China

XIE-YAN SONG,[1]

Department of Earth Sciences, The University of Hong Kong, Hong Kong, People's Republic of China and State Key Laboratory of Ore Deposit Geochemistry, Institute of Geochemistry, Chinese Academy of Sciences, Guiyang 550002, People's Republic of China

MEI-FU ZHOU, CHRISTINE YAN WANG, LIANG QI,

Department of Earth Sciences, The University of Hong Kong, Hong Kong, People's Republic of China

AND CHENG-JIANG ZHANG

College of Applied Nuclear Technology and Automation Engineering, Chengdu University of Technology, Chengdu 610059, People's Republic of China

Abstract

The Jinchuan ultramafic body on the southwestern margin of the North China craton hosts a giant Ni-Cu-(PGE) deposit. This dike-like intrusion consists mainly of lherzolite, dunite, and minor pyroxenite. Fortly-seven vol% of the intrusion is composed of disseminated sulfide ore and minor massive and net-textured ores. Ore bodies occur commonly in the lower part of the intrusion; the largest contains about 50% of the total metallic resources in Jinchuan, and has a "flame-like" shape in vertical cross-section. The ultramafic rocks have high MgO (19–45 wt%), low CaO (<6.5 wt%) and Al_2O_3 (<7 wt%), and right-inclined chondrite-normalized REE patterns. These rocks contain variable Ir (0.4–17 ppb), Ru (0.6–21 ppb), Rh (0.05–8.4 ppb), Pt (0.6–196 ppb), and Pd (1.2–135 ppb), in general lower than those in the sulfide ores (2.9–110 ppb Ir, 3.3–260 ppb Ru, 1.5–237 ppb Rh, 6.9–3972 ppb Pt, and 15–532 ppb Pd). They have high Th/Nb (0.15–0.5) ratios and show primitive mantle-normalized trace element patterns with Nb-Ta negative anomalies, consistent with derivation from mantle magmas variably contaminated by crustal materials. Compositional heterogeneity of the disseminated sulfides cannot be accounted for by in-situ fractional crystallization, but is consistent with differentiation and sulfide segregation in a staging magma chamber at depth. We propose a compressive tectonic model in which injection of sulfide-poor, crystal-rich magmas from the upper part of the staging magma chamber was followed by injection of a sulfide-rich crystal-mush from the lower part of the staging magma chamber to form the Jinchuan body.

Introduction

THE JINCHUAN Ni-Cu-(PGE) sulfide deposit on the southwestern margin of the North China craton (Fig. 1) contains 5.45 million metric tons of metallic Ni, making it the third-largest Ni-Cu sulfide deposit in the world. The host intrusion is a small dike-like body with a surface expression of less than 1.5 km^2, and was dated at 1508 Ma (Tang et al., 1992; Tang and Li, 1995) and at 800 Ma (Li et al., 2005). An important problem regarding its origin is why and how such a large amount of sulfides was concentrated within such a small ultramafic intrusion. The largest orebody in the central part of the Jinchuan intrusion has a "flame-like" vertical shape (Fig. 2). These features are unique compared to other world-class magmatic Ni-Cu sulfide deposits related to basaltic magmas—e.g., those in the Noril'sk region, Russia (Naldrett, 1999; Naldrett and Lightfoot, 1999) and the Voisey's Bay Ni-Cu-Co sulfide deposit in Canada (Naldrett, 1999; Li et al., 2000).

Prior to this study, geochemical data for the Jinchuan intrusion were sparse (e.g., Tang, 1991; Chai and Naldrett, 1992a, 1992b; Yang et al., 1998; Barnes and Tang, 1999; De Waal and Xu, 2004; Li et al., 2004) and the factors controlling S-saturation in the magma were not well understood. Here we report new major-oxide, trace element, and PGE

[1]Corresponding author; email: songxieyan@vip.gyig.ac.cn

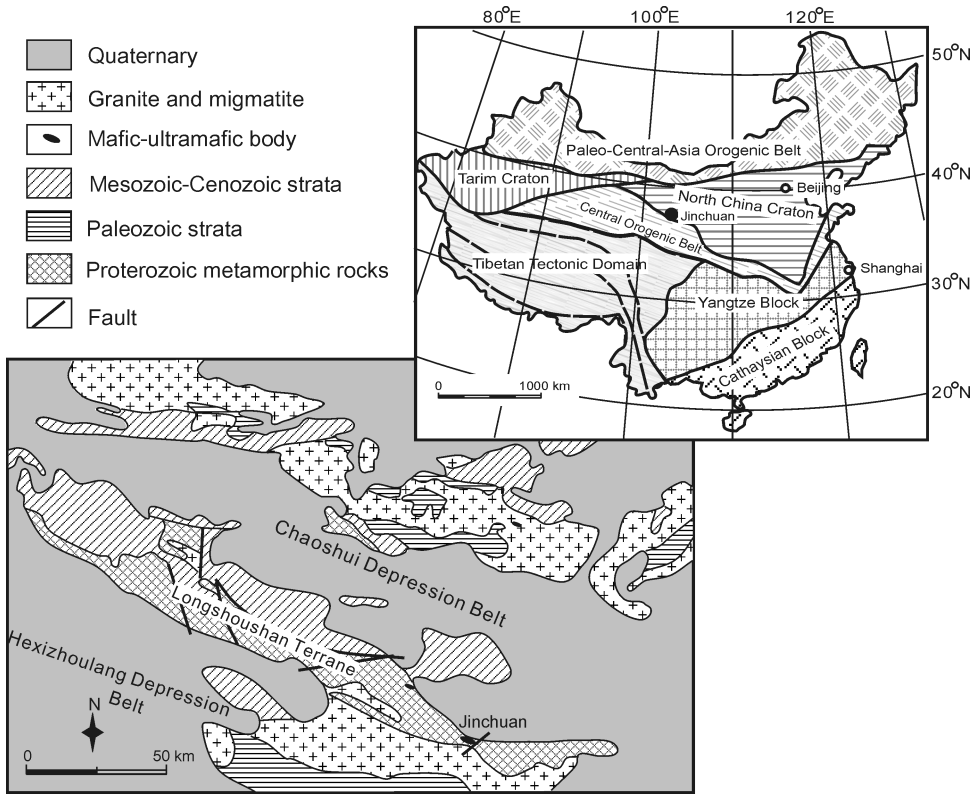

FIG. 1. Geological setting of the Jinchuan deposit. It is located in the eastern part of the Longshoushan terrane, which comprises the southwestern margin of the North China craton (modified after Zhou et al. 2002b and Tang and Barnes, 1998).

data for 33 samples from the Jinchuan intrusion. These data provide valuable insight into the processes that concentrated sulfides in this body.

Geological Background

Regional geology

The North China craton is bounded by the Central Asian Orogenic Belt to the north and the Central Orogenic Belt to the south and east (Fig. 1). It consists of the eastern and western blocks that evolved independently during the Archean and collided along the Trans–North China orogen during a Paleoproterozoic event (Zhao et al., 2005). The western block formed by amalgamation of the Ordos block in the south and the Yinshan block in the north along the E-W–trending Khondalite belt before the collision between the west and east blocks (Zhao et al., 2005). The basement of these two blocks consists of Archean to Paleoproterozoic metamorphic rocks and is unconformably overlain by Mesoproterozoic volcanic-sedimentary successions (Zhao et al., 2005).

The Longshoushan terrane is located in the southwestern margin of the Yinshan block. It comprises the Baijiazuizi and Tamazigou metamorphic complexes, which are exposed along NW-SE–trending thrust faults (Fig. 1). The Baijiazuizi complex is composed of migmatites, gneisses, and marbles, whereas the Tamazigou complex consists of schists and banded marbles. Both of these complexes are overlain by Neoproterozoic and Paleozoic conglomerate, sandstone, and limestone (Fig. 1). Numerous mafic-ultramafic intrusions, including the Jinchuan

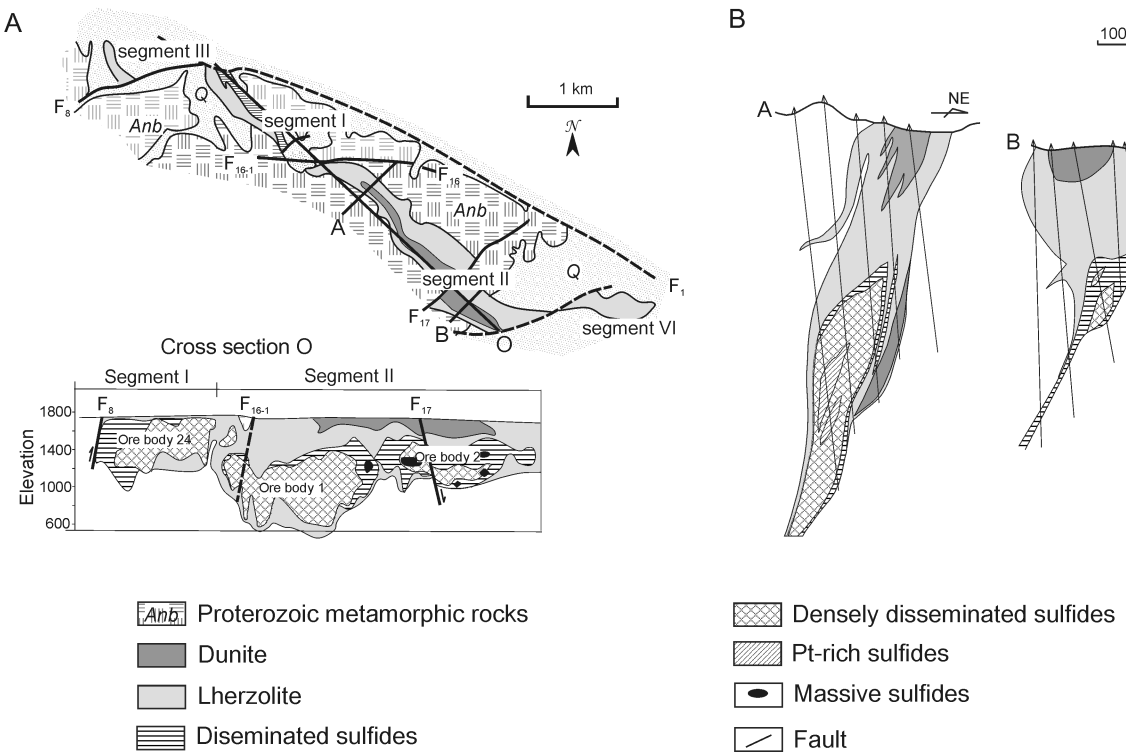

FIG. 2. Geological map of the Jinchuan intrusion after Tang and Li (1995). A. Distribution of the segments of the Jinchuan intrusion and cross-section. B. Cross-sections of ore bodies 1 and 2.

body, are hosted by the Bajiazuizi and Tamazigou complexes.

Geology of the Jinchuan intrusion

The Jinchuan body, 6500 m long and a few tens to > 500 m wide, intruded the Baijiazuizi metamorphic complex (Fig. 2). It strikes NW-SE and dips 50–80° to the southwest. The elongate body is divided into segments III, I, II, and VI from west to east by a series of NE-trending strike-slip faults. Dikes of granodiorite, lamprophyre, and diabase intrude segments along NE-trending fractures (Fig. 2). This intrusion is mainly composed of lherzolite and dunite, but contains minor pyroxenite along its margins and in the lower parts of the body. The dunite is composed dominantly of olivine, with minor plagioclase and pyroxene that may be concentrated locally. Lherzolite and pyroxenite consist of olivine and pyroxene in different proportions, with minor plagioclase, amphibole, and phlogopite. The rocks along the margins of the intrusion have been converted to tremolite-serpentine-chlorite schists because of extensive shearing.

Silicate minerals, such as olivine ($Fo_{78–86}$), orthopyroxene ($Wo_{0–10}En_{70–85}Fs_{12–28}$), and clinopyroxene ($Wo_{35–50}En_{45–58}Fs_{10–20}$), and igneous textures are locally preserved, although most of the rocks are pervasively altered (Tang and Li, 1995; Chai and Naldrett, 1992a, 1992b; De Waal and Xu, 2004; Li et al., 2004). The relict mineral chemistry suggests that the ultramafic rocks are cumulates derived from a high-Mg basaltic magma (Chai and Naldrett, 1992a, 1992b).

Geology of the sulfide ore bodies

Segment I (Fig. 2) hosts more than 200 sulfide ore bodies, of which 13 are rich in PGE (Pt + Pd >1 ppm; Tang and Li, 1995). More than 300 ore bodies have been identified in segment II, of which 38 are PGE-rich. In contrast, segments III and IV have 37 and 42 PGE-poor ore bodies, respectively. The three largest ore masses, No. 24 in segment I, and Nos. 1 and 2 in segment II, account for over 90% of the total Cu, Ni, and PGE reserves of the Jinchuan deposit (Tang and Li, 1995). The ore bodies occupy a large proportion (about 47%) of the ultramafic body.

Number 24 is a tabular-shaped body about 1500 m long and 100–200 m wide (Chai and Naldrett, 1992a, 1992b; Tang and Li, 1995) that crops out at the surface for about 600 m in its westernmost part before plunging underground toward the east. Lying in the western part of segment II, ore body 1 is hosted within lherzolite and olivine pyroxenite (Fig. 2). It is the biggest deposit and accounts for more than 50% of the total reserves of both Ni and Cu (Tang and Li, 1995). This giant ore body has a "flame-like" form and extends from a depth of about 200 m to more than 1100 m below the surface. It extends up to 1500 m along strike and has a variable width between a few tens of meters to 150 m. In contrast, body 2, 1300 m long and ~120 m wide, occurs in the eastern part of segment II. It generally marks the base ore of the intrusion and is overlain by lherzolite (Chai and Naldrett, 1992a). Massive ore bodies appear within or at the base of ore body 2 along fractures. Disseminated and net-textured sulfide deposits occur mostly in the dunite.

Ore minerals include pyrrhotite, pentlandite, violarite, chalcopyrite, and cubanite. Magnetite is ubiquitous in the rocks.

Sampling and Analytical Methods

Lherzolite, massive ore, net-textured ore, and disseminated ore from the three largest ore bodies in segments I and II were sampled. Samples were powdered using an agate mill. Sulfur was determined using a LECO analyzer in the Ontario Geoscience Laboratory, Ontario Geological Survey. Ni, Cu, and major oxides, except for SiO_2, were measured by inductively coupled plasma atomic emission spectroscopy (ICP-AES) at the Guangzhou Institute of Geochemistry, Chinese Academy of Sciences. The samples were digested with 1 ml of HF and 0.5 ml of HNO_3 in screw-top PTFE-lined stainless steel bombs at 190°C for 12 h. The precision of the analyses is generally better than 1% for elements in concentrations greater than 200 ppm, and 1–3% in specimens containing less than 200 ppm. International reference materials (GSR-1, 2, 3, 4, 5; AMN-1; OU-6; RTS-2, 3; GBPG-1; GBW-07267; GeoPT-12) were used for calibration. Trace elements, including rare-earth elements (REE) were determined by inductively coupled plasma mass spectrometry (ICP-MS) at the University of Hong Kong (HKU), using the procedure described by Qi et al. (2000). Analytical uncertainty for the trace elements was better than 10%. PGE contents were measured by ID-ICP-MS using sodium peroxide fusion and Te co-precipitation at HKU. A detailed description of this procedure was presented by Qi et al. (2004). Precision and accuracy as demonstrated by analyzing reference

TABLE 1. Chemical Compositions of the Rocks and Ores from the Jinchuan Body[1]

Segment/ ore body:	Segment I						Segment II						
Mineral/ores:	Lherzolite					Dunite	Lherzolite						Pyroxenite
Samples:	JC-2	JC-3	JC-4	JC-20	JC-5	J-11	JC-7	JC-12	JC-25	JZ-5	JZ-6	JC-9	JC-11
Major oxides, wt%													
TiO_2	0.21	0.2	0.23	0.19	0.25	0.46	0.29	0.12	0.47	0.23	0.28	0.44	0.15
Al_2O_3	2.44	2.17	2.42	3.11	2.57	4.61	3.91	1.6	6.41	3.24	1.01	6.74	0.25
Fe_2O_3	13.6	15.1	15.2	17.0	12.3	14.1	14.1	13.7	13.6	16.9	16.8	12.6	2.9
MgO	36.4	36.2	34.0	31.2	34.0	29.3	32.5	36.1	27.4	31.2	27.7	26.3	18.3
MnO	0.16	0.17	0.21	0.18	0.13	0.16	0.16	0.16	0.17	0.17	0.17	0.17	0.07
CaO	1.33	1.22	1.17	1.2	2.25	3.52	2.05	0.17	4.66	2.17	2.47	4.69	30.83
Na_2O	0.13	0.09	0.03	0.06	0.11	0.28	0.54	0.03	0.74	0.18	0.37	0.83	0.03
K_2O	0.22	0.1	0.3	0.66	0.51	0.12	0.19	0.06	0.68	0.2	0.35	0.46	0.02
P_2O_5	0.02	0.01	0.02	0.01	0.02	0.05	0.03	0.01	0.04	0.02	0.02	0.05	0
Trace elements, ppm													
Rb	7.2	2.7	22.24	44	23	3.6	5.5	0.76	23	4.3	8.4	11	0.5
Sr	19	49	8.9	9.1	8	44	37	10	73	29	61	179	165
Ba	67	39	20	45	54	28	52	24	56	39	109	259	12
Th	0.52	0.17	0.31	0.4	1.3	0.55	0.38	0.13	0.6	0.11	0.14	0.58	0.84
V	55	54	46	41	72	104	80	52	104	72	76	104	15
Cr	3150	3352	1044	1070	4018	3155	2996	4470	2313	2661	2539	2461	68
Co	128	156	100	64	139	132	120	134	122	91	116	104	29
Y	2.8	2.6	3.3	3.2	4	6.3	4.6	1.7	8.1	2	2.4	7.9	4.2
Zr	16	15	19	14	23	40	25	9.8	46	22	27	39	16
Hf	0.43	0.43	0.49	0.35	0.59	0.94	0.63	0.22	1.1	0.5	0.62	0.97	0.42
Nb	0.94	0.7	1.1	1.1	1.2	2.2	1.2	0.46	2.1	1.2	1.5	2	3.1
Ta	0.08	0.06	0.08	0.06	0.09	0.13	0.08	0.03	0.12	0.06	0.08	0.12	0.17
U	0.1	0.04	0.08	0.1	0.23	0.15	0.08	0.13	0.11	0.1	0.1	0.11	1.6
La	2.11	1.89	0.77	1.51	1.02	3.26	3.91	1.8	6.05	1.09	1.57	5.93	3.48
Ce	4.83	4.16	2.7	4.5	4.22	8.46	7.94	3.66	13.3	3.55	4	13.23	8.31
Pr	0.64	0.53	0.44	0.66	0.76	1.18	0.96	0.42	1.67	0.51	0.58	1.71	1.04
Nd	2.67	2.21	2.09	2.71	3.7	5.26	3.87	1.62	7	2.21	2.62	7.01	4.23
Sm	0.61	0.54	0.55	0.58	0.88	1.25	0.89	0.34	1.58	0.53	0.63	1.59	0.88
Eu	0.18	0.18	0.11	0.12	0.12	0.36	0.28	0.12	0.54	0.17	0.18	0.49	0.19
Gd	0.57	0.48	0.53	0.57	0.77	1.12	0.84	0.32	1.46	0.46	0.55	1.47	0.77
Tb	0.09	0.07	0.09	0.09	0.13	0.18	0.14	0.05	0.24	0.08	0.09	0.23	0.12
Dy	0.54	0.48	0.6	0.57	0.74	1.12	0.83	0.3	1.47	0.47	0.57	1.43	0.74
Ho	0.11	0.1	0.12	0.12	0.15	0.23	0.17	0.06	0.3	0.1	0.11	0.29	0.15
Er	0.32	0.29	0.35	0.33	0.44	0.65	0.5	0.19	0.87	0.26	0.33	0.84	0.44
Tm	0.05	0.05	0.05	0.05	0.06	0.09	0.07	0.03	0.12	0.04	0.04	0.12	0.06
Yb	0.3	0.28	0.34	0.33	0.4	0.59	0.45	0.18	0.78	0.23	0.27	0.78	0.38
Lu	0.05	0.04	0.05	0.05	0.06	0.09	0.07	0.03	0.12	0.03	0.04	0.12	0.05
Zr/Nb	17.0	21.4	17.3	12.7	19.2	18.2	20.8	21.3	21.9	18.3	18.0	19.5	5.2
La/Sm	3.5	3.5	1.4	2.6	1.2	2.6	4.4	5.3	3.8	2.1	2.5	3.7	4.0
Gd/Yb	1.9	1.7	1.6	1.7	1.9	1.9	1.9	1.8	1.9	2.0	2.0	1.9	2.0
Ti/Y	450	462	418	356	375	438	378	424	348	690	700	334	214

Table continues

TABLE 1. *Continued*

Segment/ore body	Segment II			Orebody 24						Orebody 1			
Rock/ores:	Pyroxenite	Diss		Net					Mass	Diss		Net	
Samples:	JC-24	JC-23	JC-26	JC-30	JC-35	JC-38	JC-39	JC-40	JC-49	JC-28	JC-29	JZ-2	JZ-4
						Major oxides, wt%							
TiO_2	0.25	0.21	0.43	0.18	0.1	0.09	0.12	0.05	0.01	0.36	0.44	0.14	0.06
Al_2O_3	3.47	1.69	6.31	1.74	2.03	1.64	1.24	0.53	0.07	4.19	5.67	0.89	1.2
Fe_2O_3	16.1	15.6	16.0	23.1	22.0	23.2	31.6	29.7	58.2	16.5	15.5	28.6	25.4
MgO	31.2	32.7	24.8	29.2	26.6	25.8	21.4	22.0	0.6	29.5	23.7	29.3	29.8
MnO	0.18	0.13	0.15	0.15	0.16	0.1	0.18	0.08	0	0.18	0.19	0.14	0.15
CaO	2.54	2.06	4.26	1.16	0.22	0.44	0.88	0.05	0.06	3.5	5.12	0.56	1.07
Na_2O	0.32	0.06	0.54	0.03	0.01	0.03	0.02	0.01	0.01	0.5	0.73	0.04	0.07
K_2O	0.24	0.28	0.49	0.26	0.08	0.06	0.06	0.04	0.04	0.38	0.79	0.15	0.12
P_2O_5	0.01	0.01	0.04	0	0	0	0	0	0	0.03	0.04	0	0
						Trace elements, ppm							
Rb	5.2	11	13	15	1.8	0.98	0.71	0.27	0.34	10	25	3.7	2.6
Sr	85	7.3	71	11	4.5	5.7	13	3	1.3	77	97	9.7	27
Ba	74	21	116	16	9.2	4.7	11	3.57	2.89	195	579	35	28
Th	0.35	0.86	0.75	0.3	0.18	0.11	0.04	0.07	0.03	0.59	0.94	0.05	0.04
V	75	48	101	25	39	47	73	37	2.7	83	98	48	29
Cr	2847	3367	2308	722	1966	2277	4080	2123	86	2590	2050	3461	1601
Co	163	193	67	344	405	411	569	452	1412	135	173	457	411
Y	4.3	3	8.2	2.7	2.5	1.9	1.4	0.87	0.09	5.4	9.3	0.99	0.98
Zr	22	24	43	14	13	5.6	5	4.7	0.71	34	56	7.3	5.2
Hf	0.58	0.59	1.1	0.32	0.29	0.18	0.16	0.11	0.05	0.89	1.4	0.12	0.09
Nb	1.1	1.2	2.1	1.4	0.28	0.15	0.14	0.07	0.05	1.7	2.7	0.85	0.14
Ta	0.06	0.08	0.12	0.07	0.03	0.01	0.01	0.01	0.004	0.1	0.17	0.03	0.01
U	0.08	0.2	0.17	0.08	0.02	0.02	0.01	0.01	0.02	0.12	0.26	0.07	0.01
La	3.15	0.67	5.45	1.68	0.82	0.86	0.6	0.39	0.05	3.65	4.67	0.79	0.57
Ce	6.46	2.75	13.71	4.77	2.51	2.58	1.36	0.85	0.12	8.23	12.89	2.09	1.39
Pr	0.83	0.5	1.84	0.66	0.37	0.34	0.2	0.1	0.01	1.09	1.73	0.29	0.17
Nd	3.42	2.48	7.42	2.71	1.63	1.35	0.9	0.42	0.07	4.53	7.35	1.23	0.66
Sm	0.78	0.63	1.68	0.57	0.46	0.33	0.23	0.09	0.02	1.05	1.75	0.33	0.17
Eu	0.25	0.08	0.55	0.11	0.13	0.15	0.08	0.05	0.003	0.32	0.46	0.07	0.07
Gd	0.75	0.53	1.5	0.51	0.47	0.31	0.23	0.1	0.01	0.99	1.65	0.25	0.18
Tb	0.12	0.09	0.24	0.08	0.08	0.05	0.04	0.02	0.002	0.16	0.27	0.04	0.03
Dy	0.75	0.54	1.49	0.49	0.51	0.33	0.25	0.12	0.01	0.99	1.64	0.23	0.19
Ho	0.16	0.12	0.31	0.1	0.1	0.07	0.05	0.03	0.002	0.2	0.34	0.05	0.04
Er	0.46	0.33	0.9	0.3	0.27	0.21	0.16	0.09	0.01	0.57	1.01	0.13	0.12
Tm	0.07	0.04	0.12	0.04	0.04	0.03	0.02	0.01	0.001	0.08	0.15	0.02	0.02
Yb	0.43	0.3	0.77	0.26	0.25	0.2	0.15	0.1	0.01	0.53	0.93	0.12	0.12
Lu	0.07	0.05	0.12	0.04	0.04	0.03	0.02	0.02	0.001	0.08	0.14	0.02	0.02
Zr/Nb	20.0	20.0	20.5	10.0	46.4	37.3	35.7	67.1	14.2	20.0	20.7	8.6	37.1
La/Sm	4.0	1.1	3.2	2.9	1.8	2.6	2.6	4.3	2.5	3.5	2.7	2.4	3.4
Gd/Yb	1.7	1.8	1.9	2.0	1.9	1.6	1.5	1.0	1.0	1.9	1.8	2.1	1.5
Ti/Y	349	420	315	400	240	284	514	345	667	400	284	848	367

Table continues

TABLE 1. *Continued*

Segment/ore body:	Orebody 1		Orebody 2				
Rock/ores:	Mass	Diss	Net				Mass
Samples:	JC-47	JC-58	JC-32	JC-34	JC-54	JZ-11	JZ-15
			Major oxides, wt%				
TiO_2	0.01	0.14	0.13	0.12	0.31	0.12	0.01
Al_2O_3	0.15	3.23	0.76	2.34	4.41	0.86	0.03
Fe_2O_3	55.6	23.7	32.7	19.1	18.7	38.7	70.9
MgO	0.5	18.0	21.7	31.7	28.0	19.7	0.3
MnO	0.01	0.15	0.11	0.16	0.2	0.22	0.01
CaO	0.07	9.3	0.07	2.12	2.78	0.59	0.31
Na_2O	0.02	0.04	0.02	0.2	0.52	0.01	0
K_2O	0.05	0.06	0.09	0.22	0.39	0.05	0.04
P_2O_5	0	0.01	0	0.01	0	0	0
			Trace elements, ppm				
Rb	0.43	0.8	1.6	6.1	11	0.42	0.16
Sr	6.6	273	8.73	43	125	10	4.3
Ba	7.7	9.8	31	97	193	3.9	3.7
Th	0.03	0.85	0.1	0.2	0.36	0.03	0.004
V	6.06	68	63	48	78	72	32
Cr	146	2575	2263	2978	2720	2443	29
Co	1224	398	435	222	108	452	1000
Y	0.14	6.2	0.87	2.9	4.7	0.97	0.03
Zr	1.1	53	6.3	11	24	4.6	0.49
Hf	0.04	1.3	0.17	0.33	0.59	0.08	0
Nb	0.09	1.5	0.3	0.81	1.5	0.07	0.52
Ta	0.005	0.11	0.03	0.04	0.08	0.01	0.02
U	0.01	0.11	0.03	0.06	0.08	0.01	0.01
La	0.19	4.91	0.84	1.55	3.77	0.22	0.19
Ce	0.48	9.09	1.78	3.71	8.76	0.58	0.41
Pr	0.05	1.14	0.22	0.46	1.1	0.09	0.04
Nd	0.22	4.82	0.95	1.97	4.45	0.44	0.11
Sm	0.04	1.19	0.21	0.5	0.92	0.11	0.02
Eu	0.01	0.25	0.05	0.18	0.35	0.04	0.01
Gd	0.03	1.22	0.18	0.5	0.91	0.11	0.01
Tb	0.005	0.21	0.03	0.08	0.14	0.02	0.001
Dy	0.02	1.22	0.16	0.5	0.82	0.13	0.01
Ho	0.005	0.24	0.03	0.11	0.17	0.03	0.001
Er	0.01	0.65	0.1	0.3	0.5	0.1	0.003
Tm	0.002	0.08	0.01	0.05	0.07	0.02	0
Yb	0.01	0.52	0.11	0.28	0.44	0.12	0.002
Lu	0.001	0.08	0.02	0.04	0.07	0.02	4E-04
Zr/Nb	12.2	35.3	21.0	13.6	16.0	65.7	0.9
La/Sm	4.8	4.1	4.0	3.1	4.1	2.0	9.5
Gd/Yb	3.0	2.3	1.6	1.8	2.1	0.9	5.0
Ti/Y	429	135	897	248	396	742	2000

[1]Abbreviations: Diss = disseminated ore; Net = net-textured ore; mass = massive ore.

materials, such as UMT-1 and WPR-1, are better than 10% (Tables 1 and 2). PGE contents of the blank are generally smaller than 1 ppb: Ir < 0.15 ppb, Ru < 0.15 ppb, Rh < 0.05 ppb, Pt < 0.5 ppb, and Pd < 0.5 ppb.

Analytical Results

Major-oxide contents of the Jinchuan intrusive rocks and ores are presented in Table 1. All samples exhibit large losses on ignition due to hydrothermal alteration. Concentrations of Fe_2O_3 and Ni can be elevated significantly in samples in which even small amounts of sulfides are present in the rocks and ores. In order to examine the variation in the silicate component of the rocks and the magmatic evolution, it was necessary to recalculate the chemical compositions of the silicate portion (mixture of mafic minerals and magma) on a sulfide-free basis, and the sulfide melts using the following procedure (Song, 2004).

1. Composition of sulfide liquid: assume that all Cu, Zn, and Ni combined with S and formed sulfide melts, which solidified to chalcopyrite ($CuFeS_2$), sphalerite (ZnS), and pentlandite ($(Fe_{4.5}Ni_{4.5})S_8$. Excess S would combine with Fe to form pyrite (FeS_2), and any extra Fe would remain in the silicate magma in the form of Fe_2O_3.

2. Composition of silicate portion: recalculate the oxide percentages using the other oxides and the extra Fe_2O_3 after subtracting the iron in the sulfides.

3. Assume that all PGE enter sulfide melts because of their extremely high partition coefficients between sulfide melt and silicate melt (Peach et al., 1990).

4. Assume that all incompatible elements remain in the silicate portion.

Major and trace elements

Similar to the observations of Chai and Naldrett (1992a, 1992b), the new data indicate that the silicate parts of all the Jinchuan rocks and ores are rich in MgO (19–45 wt%) and low in CaO and Al_2O_3 (mostly < 6.5 wt% and < 7 wt%, respectively). As shown in Figure 3, rocks in segments I and II have similar chemical compositions, although samples of segment II have wider compositional variations. Contents of CaO, TiO_2, Na_2O, and P_2O_5 of all Jinchuan sulfide-poor rocks from which sulfides have been subtracted show a positive correlation with Al_2O_3 , whereas MgO and Cr correlate negatively with Al_2O_3 (Fig. 3). These correlations indicate that chemical variations in the silicate magma were controlled by fractionation of olivine and chromite. Recalculated contents of oxides in the silicate portions of the ore samples overlap those of the sulfide-poor rocks. However, the silicate portions of some ores have high contents of CaO, TiO_2, Al_2O_3, and Na_2O compared to the sulfide-poor rocks (Fig. 3).

The silicate portions of the rocks and ores in segment II have larger variations in high-field-strength elements (HFSE) and rare-earth elements (REE) than those in segment I (Table 1 and Fig. 4). Concentrations of the HFSE and REE increase with increasing Al_2O_3, indicating that they were concentrated in residual silicate melts during fractional crystallization. The silicate portions of a few ores contain higher contents of HFSE and REE than the sulfide-poor rocks (Fig. 4). Most of the rocks show relatively smooth chondrite-normalized REE patterns, with LREE enrichment (1–6 ppm La and 0.5–1.6 ppm Sm). A few samples from segment I show small negative Eu anomalies (Fig. 5). The HREE contents of these rocks are only slightly lower than the MREE contents, and the Gd/Yb ratios are mostly less than 2.0 (Table 1). Figure 5 also shows that REE contents of the silicate portions of the disseminated ores are similar to, or higher than, those of the sulfide-poor rocks.

The concentrations of selected trace elements of the Jinchuan samples normalized to primitive mantle concentrations are shown in Figure 6. Rocks of segment II display larger variations, particularly of large-ion lithophile elements (LILE), and more obvious negative Nb-Ta anomalies than those from segment I. The silicate portions of the ores exhibit wide variations of trace element abundances. Some of the ores have relatively high contents of incompatible elements, and these have trace element patterns similar to those of the silicate rocks. Other ores have widely varying LILE and LREE contents (Fig. 6).

Platinum-group elements

Ultramafic rocks from segments I and II have large ranges of PGE contents, 0.4–17 ppb Ir, 0.6–21 ppb Ru, 0.05–8.4 ppb Rh, 0.6–196 ppb Pt, and 1.2–135 ppb Pd (Table 2). The PGE contents of the sulfide ores are typically higher than those of the sulfide-poor rocks 2.9 to 110 ppb Ir, 3.3 to 260 ppb Ru, 1.5 to 237 ppb Rh, 6.9 to 3972 ppb Pt, and 15 to 532 ppb Pd. Almost all the PGEs were concentrated in the sulfides because of their very high sulfide melt/silicate melt partition coefficients

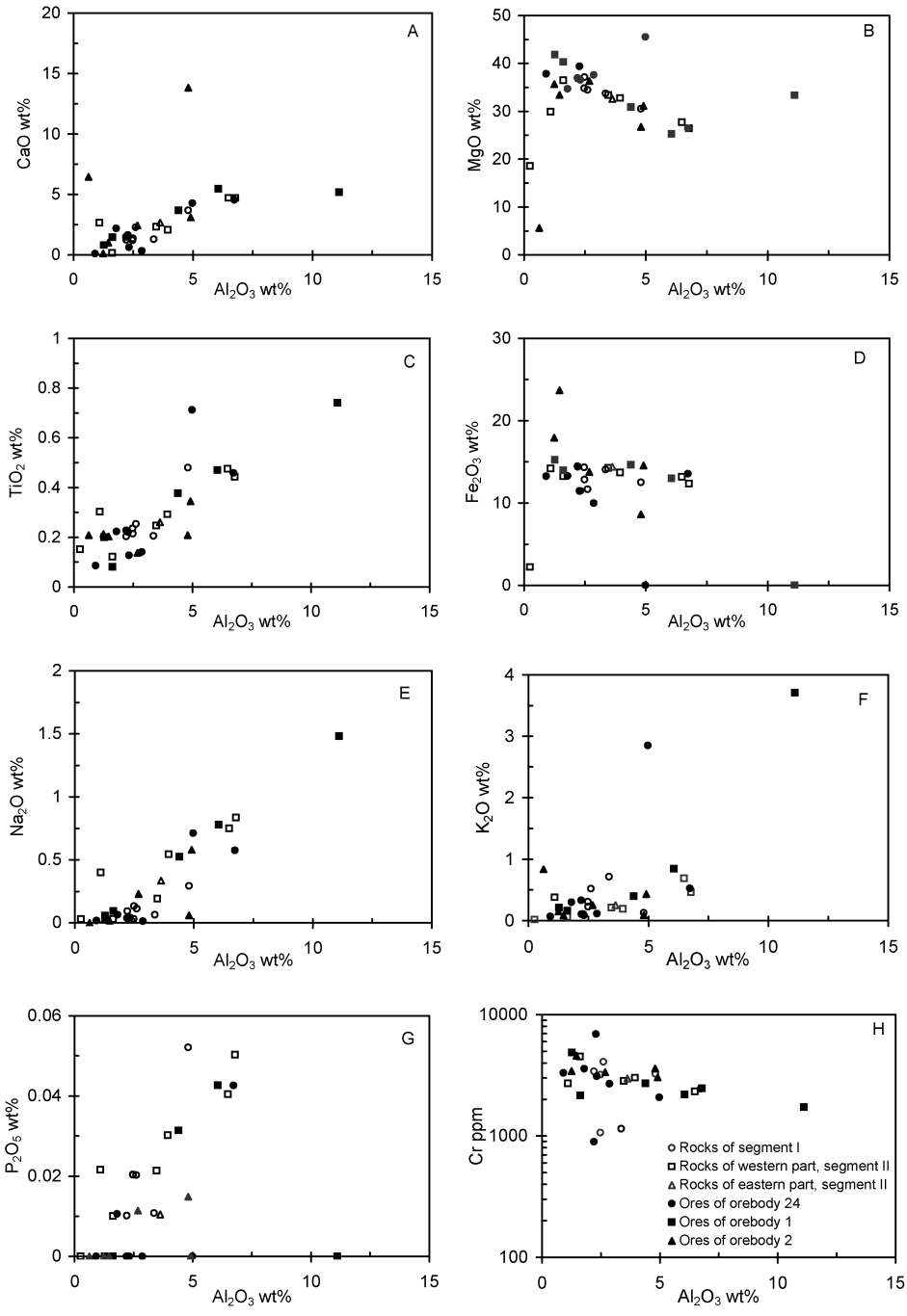

FIG. 3. Diagrams of oxides versus Al_2O_3, showing chemical variations in the silicate portions of both the sulfide-poor rocks and the ores from the Jinchuan body. Sulfides were subtracted from the compositions of rocks and ores by the method described in the text.

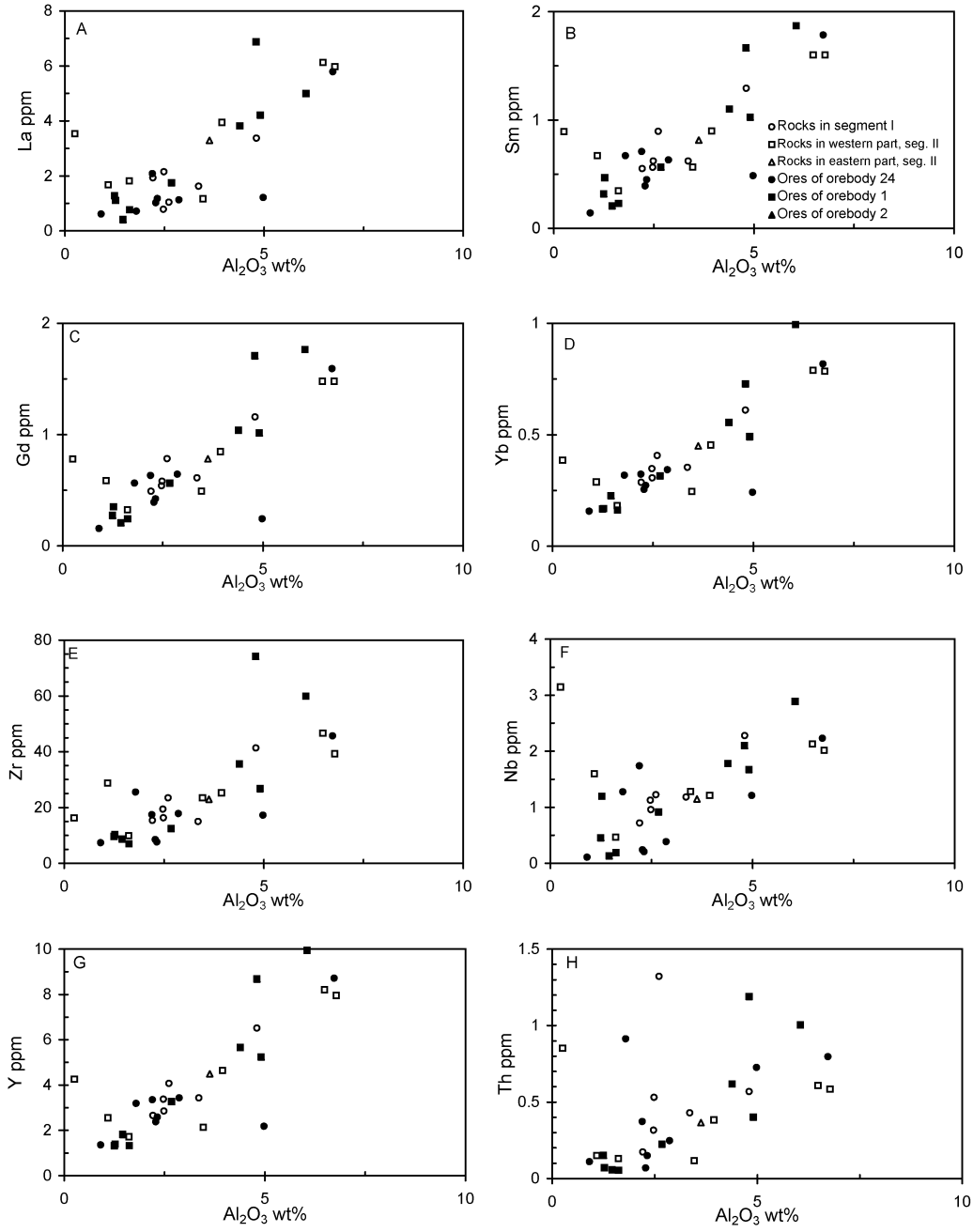

FIG. 4. Diagrams of trace elements versus Al_2O_3, demonstrating the correlations between trace elements and Al_2O_3 in the silicate portions of both sulfide-poor rocks and ores of the Jinchuan body.

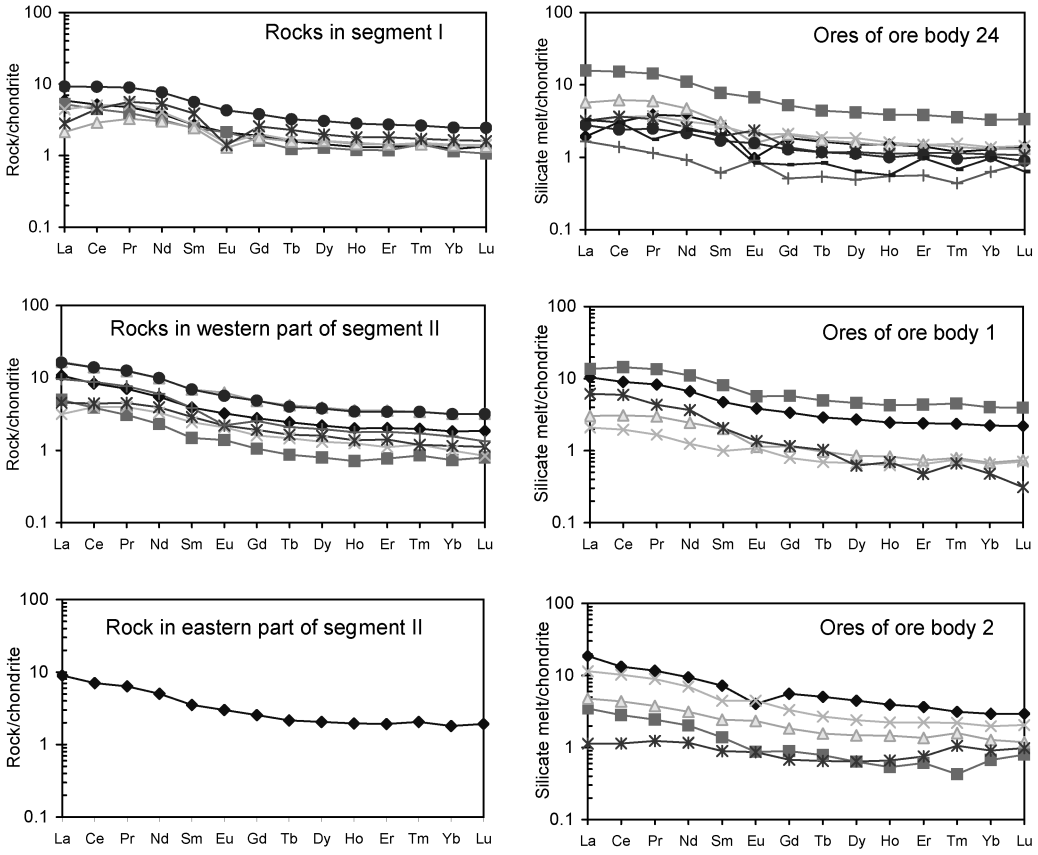

FIG. 5. Chondrite-normalized REE patterns of the sulfide-poor rocks and ores in segments I, II, and III. Chondrite values are from Taylor and MeLennan (1985).

(~103–105) (Peach et al., 1990). However, the PGE contents of sulfides in the ores are not absolutely higher than those of sulfides in the ultramafic rocks (Fig. 7). The sulfides in the silicate rocks have obviously higher Ni contents than those in the ores.

Except for Pt, the PGE concentrations in ore body 2 are lower than those in ore bodies 1 and 24. Figure 7 shows that PGE concentrations in the sulfide ores correlate positively with Ni contents. In segment I, PGEs in the sulfides of the ultramafic rocks also correlate positively with Ni, whereas in segment II they show a negative correlation (Fig. 7). This implies that the ultramafic rocks in the segments I and II underwent different processes of evolution. Ru and Rh in both rocks and ores show perfect correlations with Ir (Fig. 8), suggesting these elements behave in a similar manner during the magmatic processes.

Sulfides in both the ultramafic rocks and ores have similar primitive mantle-normalized PGE patterns, being weakly depleted in IPGE relative to PPGE (Fig. 9). Some ores show obviously negative Pt anomalies. These characteristics of the Jinchuan ores are comparable with those of the Sudbury ores, and are distinctly different from those of the Merensky Reef and UG-2 Reef of the eastern Bushveld layered intrusion, which are IPGE rich (Fig. 9). The PGE contents of the Jinchuan ores are much lower than those of the Noril'sk deposits, although they have similar PGE patterns (Fig. 9).

Discussion

Previous genetic models for the Jinchuan intrusion

As described above, the Jinchuan intrusion is quite different from other mafic-ultramafic intrusions

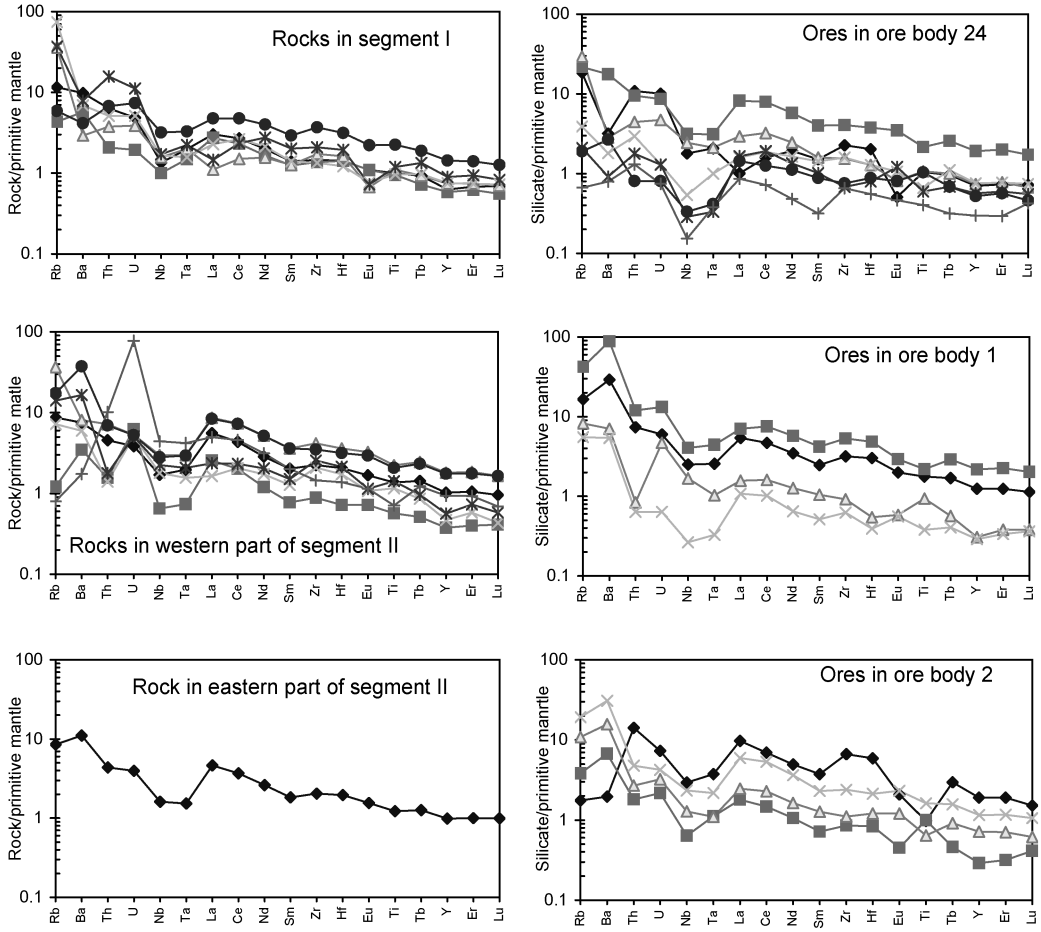

FIG. 6. Primitive mantle–normalized spider diagrams of trace elements of sulfide-poor rocks and ores in segments I, II, and III. Primitive mantle values are from Hofmann (1988).

hosting world-class Ni-Cu-(PGE) sulfide deposits, such as the Sudbury Igneous Complex and the Noril'sk sill-like intrusions, Russia (Lightfoot and Naldrett, 1999). First, the Jinchuan intrusion lacks mafic varieties, and consists entirely of ultramafic rocks without any mafic varieties, with only minor troctolite locally along marginal zones. Second, the small dike-like body is heavily sulfide-mineralized (up to 47 vol%). Finally, the largest sulfide orebody (No. 1) has a "flame-like" shape and occurs in the central part of segment II. Thus, it is difficult to interpret the formation of the Jinchuan deposit using genetic models developed elsewhere.

Tang and coworkers (Tang, 1991; Tang and Li, 1995) proposed that the Jinchuan intrusion resulted from emplacement of four magma pulses and sulfide melts. According to this model, an ultramafic magma derived from the upper mantle differentiated and formed compositional zones in a staging magma chamber at depth. The uppermost zone was thought to be composed of sulfide-poor and crystal-free magma, whereas the middle zone consisted of olivine- and pyroxene-bearing melt and the lower zone of sulfide-bearing magma. The sulfide-poor and crystal-bearing magmas were squeezed out early and formed the sulfide-poor lherzolite in the Jinchuan body or other sulfide-poor intrusions elsewhere in the Loangshoushan terrane. Then, the sulfide-bearing magmas were intruded and formed disseminated and net-textured ore bodies in the Jinchuan body. Finally, sulfide melts intruded along fractures in the eastern part of segment II to form the

TABLE 2. Nickel, Cu, PGE, and S Contents of the Rocks and Ores of the Jinchuan Body[1]

Segment/ ore body:	Segment I						Segment II				
Rock:	Lherzolite					Dunite	Lherzolite				
Sample:	JC-2	JC-3	JC-4	JC-20	JC-5	J-11	JC-7	JC-12	JC-25	JZ-5	JZ-6
S, ppm	5160	5712	5565	18739	4920	1355	1303	201	3227	17627	16731
Ni, ppm	2365	3217	2744	7082	2375	1233	1231	1384	1908	5578	5560
Cu, ppm	802	1590	556	1503	1561	187	257	71	615	2019	741
Ir, ppb	6.4	13.9	1.2	10	3.8	3	0.48	2.3	0.91	17	18
Ru, ppb	6.3	13.8	2.3	11	4.5	2	1.1	0.63	1.5	21	19
Rh, ppb	3	7.2	2.4	6.1	2.4	0.72	0.29	0.05	0.49	8.4	8.1
Pt, ppb	51	196	176	74	58	16	3.9	0.6	6.3	131	169
Pd, ppb	39	97	89	73	33	13	3.5	1.2	5.4	135	91
Ni/Cu	2.95	2.02	4.94	4.71	1.52	6.59	4.79	19.49	3.10	2.76	7.50
Pd/Ir	6.09	6.98	74.17	7.30	8.68	4.33	7.29	0.52	5.93	7.94	5.06

Segment/ore body:	Segment II		Orebody 24								
Rock:	Pyroxenite		Diss			Net					Mass
Sample:	JC-9	JC-11	JC-24	JC-23	JC-26	JC-30	JC-35	JC-38	JC-39	JC-40	JC-49
S, ppm	544	4388	13379	17338	16328	56075	84554	80771	123005	109022	295089
Ni, ppm	1036	1096	3335	5977	6796	16220	18088	19160	24222	19734	65388
Cu, ppm	203	1471	3146	4155	2101	4886	18552	14388	10415	11286	15742
Ir, ppb	0.43	0.71	16	25	13	7.6	13	17	110	12	89
Ru, ppb	0.86	1.6	14	25	19	20	19	20	122	31	260
Rh, ppb	0.3	0.65	8.3	12	11	15	17	16	44	15	237
Pt, ppb	1.7	12	74	282	114	336	37	37	33	9	55
Pd, ppb	2.4	14	71	134	138	268	222	219	318	168	532
Ni/Cu	5.10	0.75	1.06	1.44	3.23	3.32	0.97	1.33	2.33	1.75	4.15
Pd/Ir	5.58	19.72	4.44	5.36	10.62	35.26	17.08	12.88	2.89	14.00	5.98

Segment/ore body	Orebody 1					Orebody 2					
Rock	Diss		Net		Mass	Diss	Net				Mass
Sample:	JC-28	JC-29	JZ-2	JZ-4	JC-47	JC-58	JC-32	JC-34	JC-54	JZ-11	JZ-15
S, ppm	12778	20059	84866	77870	283302	84874	101490	33069	33356	155317	332632
Ni, ppm	5009	5285	19728	16825	55447	16191	17616	7979	5511	20718	50778
Cu, ppm	1887	5586	5434	11032	21254	5319	4466	1777	8231	44588	28086
Ir, ppb	3.8	3.2	37	56	46	19	6	44	2.9	19	8.1
Ru, ppb	5.3	4.9	26	67	23	23	6.1	28	3.3	17	4.5
Rh, ppb	2.5	5.8	22	41	26	17	3.3	14	1.5	7	7.6
Pt, ppb	35	70	6.9	3972	10	70	20	47	79	7.1	19
Pd, ppb	30	57	128	165	109	60	28	57	15	42	46
Ni/Cu	2.65	0.95	3.63	1.53	2.61	3.04	3.94	4.49	0.67	0.46	1.81
Pd/Ir	7.89	17.81	3.46	2.95	2.37	3.16	4.67	1.30	5.17	2.21	5.68

[1]Abbreviations: Diss = disseminated ore; net = net-textured ore; mass = massive ore.

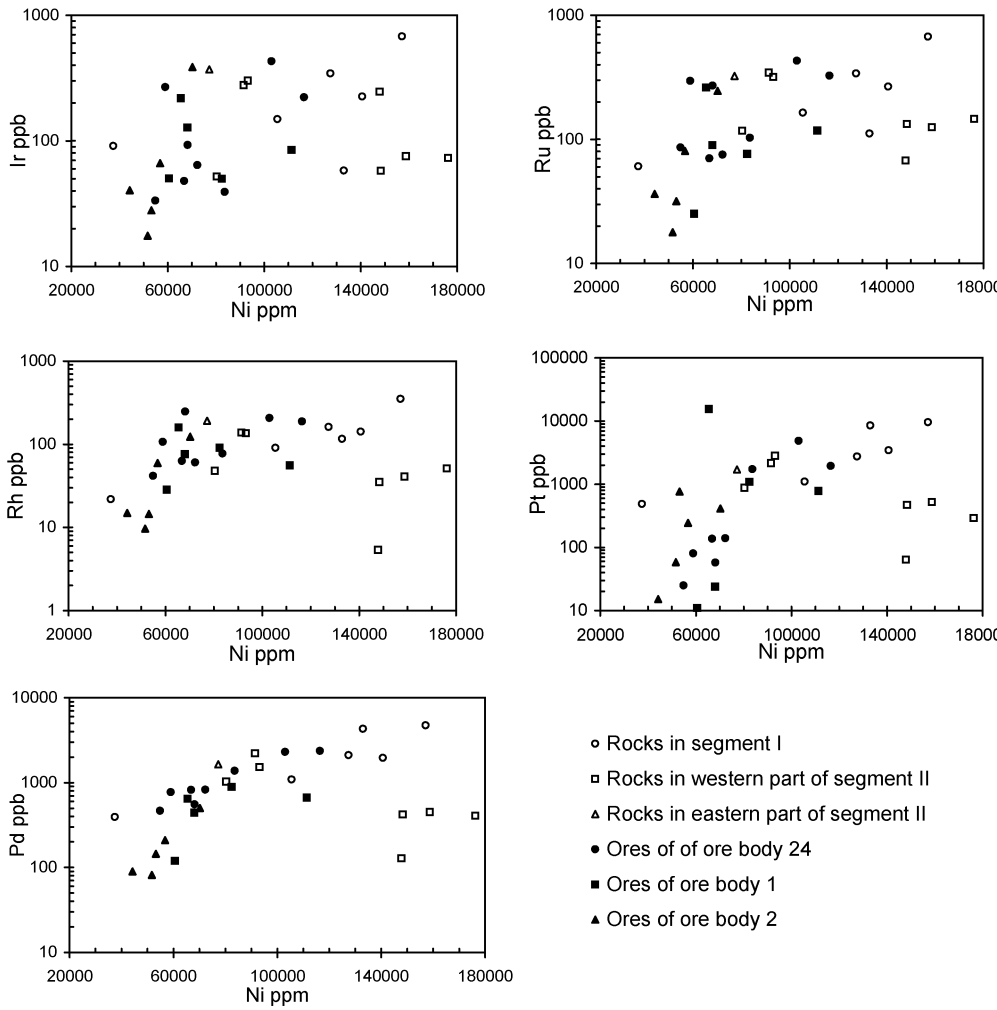

FIG. 7. Diagrams of PGE against Ni in sulfides of both sulfide-poor rocks and ores of the Jinchuan intrusion.

massive ore bodies. This model provided an explanation for the distribution of the rock phases and the ore deposits and the high proportion of sulfide mineralization in the Jinchuan intrusion.

On the other hand, Chai and Naldrett (1992a, 1992b) argued that the Jinchuan intrusion represents the root of a large layered intrusion produced by *in situ* differentiation, the upper part of the body having been eroded. In this model, the metal enrichment in ore bodies 1, 2, and 24 is thought to have resulted from interaction of early-formed sulfide liquid in a conduit with new surges of fresh magma using the same conduit. The low PGE contents in ore body 2 are thought to reflect further sulfide segregation of PGE-poor magma. According to this model, the sulfides would have concentrated in the base of the Jinchuan intrusion, where MgO was extremely high and Al_2O_3 and alkalis were low relative to the overlying zones because of accumulation of olivine and chromite.

Evaluation of the crustal contamination model

Material exchange between melts and crustal rocks is common, as basaltic magmas migrate upward from their mantle sources (Hawkesworth et al., 1984; Mahoney, 1988; Carlson, 1991; Hergt et al., 1991). In particular, crustal contamination is thought to play an important role in S-saturation of

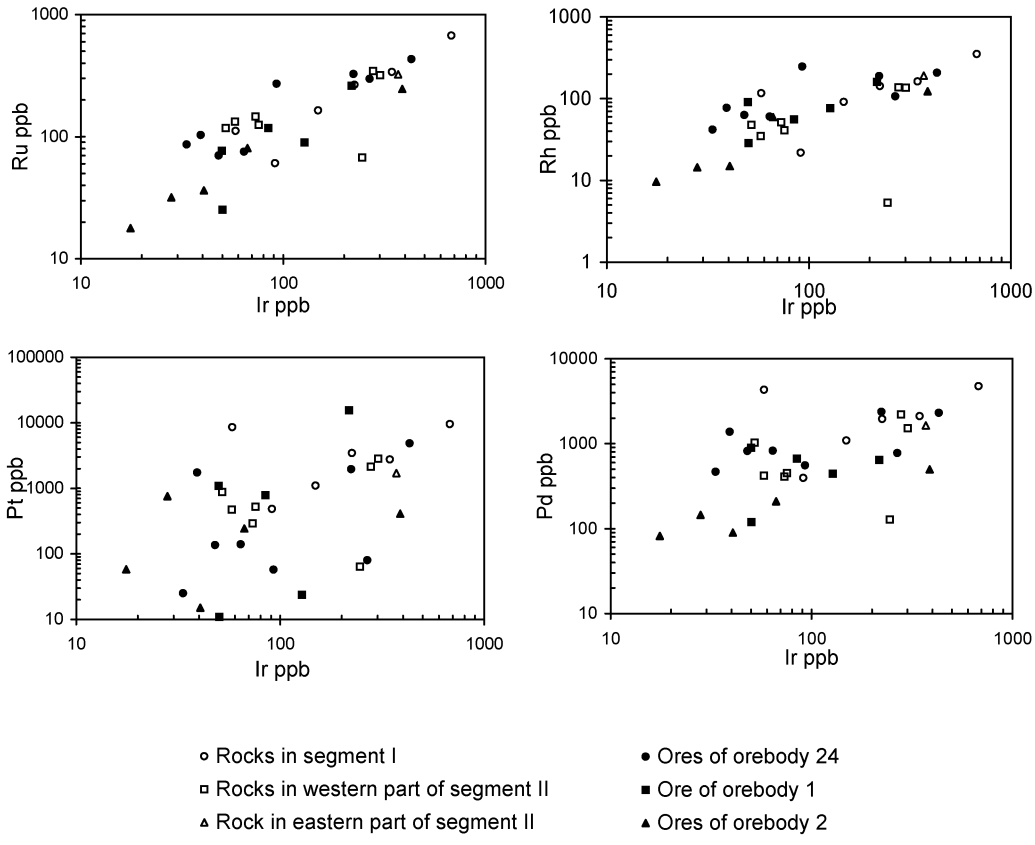

Fig. 8. Diagrams of PGE against Ir in sulfides of both sulfide-poor rocks and ores of the Jinchuan intrusion.

basaltic magmas and Ni-Cu-PGE sulfide concentration (Lightfoot et al., 1990, 1993, 1994; Naldrett et al., 1992, 1995; Brugmann et al., 1993; Wooden et al., 1993; Hawkesworth et al., 1995). However, the role of crustal contamination in the S-saturation for the formation of the Jinchuan Ni-Cu-(PGE) sulfide deposit was not evaluated in the previous studies.

Strongly incompatible elements, particularly HFSE such as Zr, Th, and REE, tend to concentrate in residual melts during fractional crystallization of mafic silicates in a closed magma system, while the ratios between them remain constant. In contrast, in an open magma system, material exchange between the magma and wallrocks can change the ratios of various incompatible elements. Thus, theoretically, the ratios of HFSE in mafic igneous rocks may be indicative of crustal contamination. The ultramafic rocks in the Jinchuan body are composed essentially of mafic minerals, sulfides, and metallic oxides (e.g., magnetite, chromite, and ilmenite). Tantalum and Nb are compatible in these oxides. Thus, the ultramafic rocks of the Jinchuan intrusion should have very low Th/Ta and Th/Nb ratios. However, most of the sulfide-poor ultramafic rocks and sulfide ores have Th/Ta and Th/Nb ratios of 2.5–6.5 and 0.15–0.6, respectively, distinctly higher than those of primitive mantle (Th/Ta = 2.3, Th/Nb = 0.15). The high Th/Ta and Th/Nb values suggest that the magmas not only experienced fractional crystallization, but also assimilated crustal materials before they reached the Jinchuan chamber (Fig. 10). Thus, the high HFSE and LILE contents and the negative Nb-Ta anomalies of the sulfide-poor rocks and sulfide ores shown in the primitive mantle–normalized trace element patterns all indicate significant crustal contamination (Fig. 6). We conclude, there-

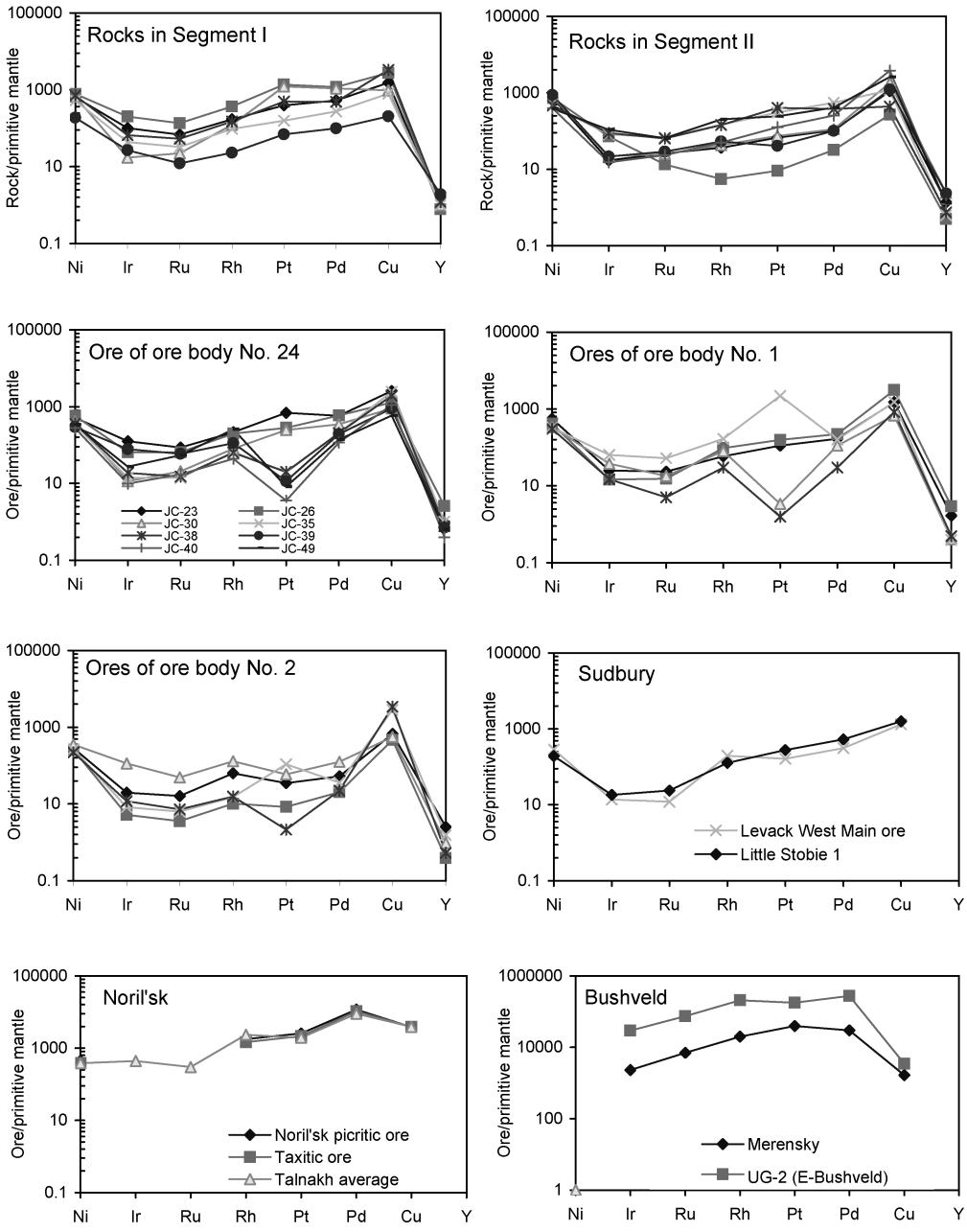

FIG. 9. Primitive mantle–normalized PGE patterns in sulfide from rocks and ores of segments I, II, and III. Primitive mantle values are from Barnes et al. (1994), PGE values of Noril'sk-Talnakh are from Naldrett and Lightfoot (1999), and those for the Merensky reef and UG-2 reef are from Hiemstra (1996) and von Gruenewaldt et al. (1986), respectively.

fore, that assimilation–fractional crystallization processes (AFC) occurred in a staging magma chamber at depth.

Both crustal contamination and fractional crystallization may increase SiO_2, decrease FeO, and reduce sulfide solubility in basaltic magmas

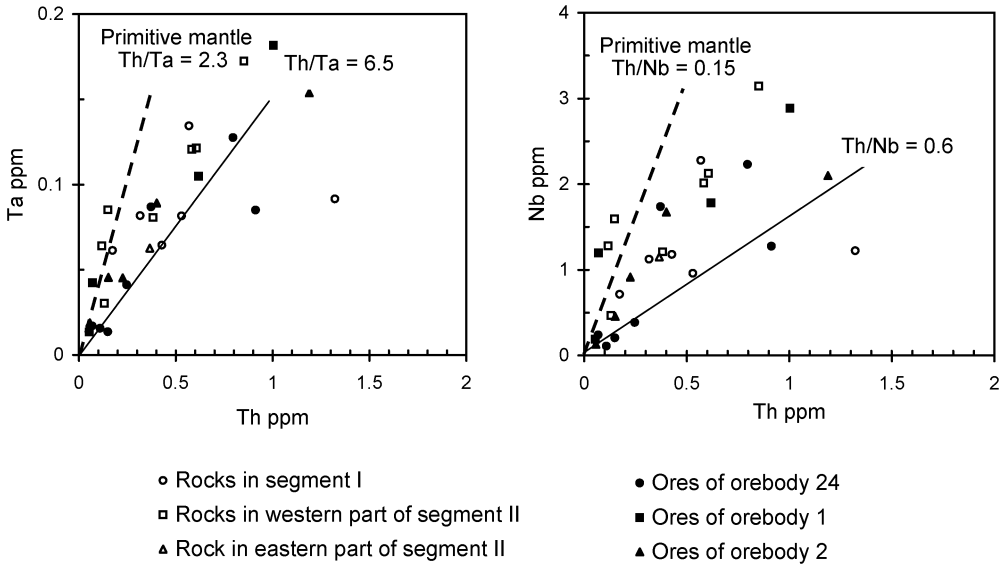

FIG. 10. Diagrams of Ta against Th and Nb against Th for rocks from the Jinchuan intrusion, employing primitive mantle values from Hofmann (1988).

(Haughton et al., 1974; Irvine, 1975; Naldrett, 1989; Keays, 1995; Li et al., 2001). Extremely low PGE and Ni abundances in flood basalts of the Siberian Traps in the Noril'sk area are attributed to sulfide segregation triggered by AFC processes in the lower crust (Arndt et al., 2003). In addition, it has been shown that the introduction of external sulfur and volatiles (e.g., CO_2 and H_2O) during crustal contamination played a role in sulfide immiscibility in the Yangliuping Ni-Cu-(PGE) sulfide deposit in the Emeishan Large Igneous Province, Southwest China (Song et al., 2003). Similarly, crustal contamination in a staging chamber is considered to have been an important factor in the sulfide immiscibility and segregation during the formation of the Jinchuan deposit.

Integrated Genetic Model for the Jinchuan Intrusion and Its Giant Ore Bodies

The "flame-like" shape of ore body 1 in segment II cannot be easily interpreted as a result of *in situ* fractional crystallization and sulfide segregation. The narrow compositional range of olivine (Fo = 79–86) in the different rocks suggest that fractional crystallization of olivine occurred in a staging magma chamber at depth, producing a stratified body of melt (De Waal and Xu, 2004; Li et al., 2004). The concentration of sulfides in the central and lower parts of segment II suggests that both flow differentiation and gravitational settling played an important role in the formation of the ore bodies (Li et al., 2004).

Our new data indicate that the silicate portions of the disseminated and net-textured sulfide ores are similar compositionally to the ultramafic rocks, but have larger chemical variations (Figs. 3 and 4). The silicate portions of some sulfide ore samples possess even higher trace-element abundances than the sulfide-poor ultramafic rocks (Fig. 6). In addition, the main ore bodies have highly variable proportions and grain sizes of rock-forming silicate minerals (Tang and Li, 1995). We interpret these phenomena to indicate that some sulfide-poor melts in the upper part of the differentiated staging magma chamber were incorporated into the sulfide-bearing crystal-mush as the mush was squeezed out to form the Jinchuan ore deposits. Lithological relationships between the silicate rocks and the sulfides, together with phase-equilibrium calculations indicate that this staging chamber was at a depth of 4–9 km, where crystallization of olivine and orthopyroxene and sulfide immiscibility occurred (De Waal and Xu, 2004). Yang et al. (1998) studied the composi-

tions of polyphase inclusions within chromite and olivine crystals and estimated that the staging chamber was 12.5 to 15 km deep.

Thus, we propose that the ultramafic rocks and ore bodies of the Jinchuan intrusion were produced by sequential injection of sulfide-poor and sulfide-bearing crystal-mush formed in a staging magma chamber. There, an S-undersaturated, high-Mg tholeiitic magma derived from the upper mantle experienced extensive AFC processes. The magma reached S-saturation because of an increase in SiO_2 and decrease in FeO and MgO during fractional crystallization of mafic minerals and assimilation of felsic crustal rocks. Olivine crystals and sulfide droplets that attracted PGE and chalcophile elements from the silicate magma settled to the base of the staging chamber. In the latter, three layers were formed from the top downward: sulfide-poor, crystal-free magmas; sulfide-poor crystal-mush; and sulfide-rich crystal-mush. The sulfide-poor magmas may have been emplaced to form sulfide-poor mafic-ultramafic intrusions/volcanic rocks elsewhere in the Longshoushan terrane. Then the sulfide-poor, crystal-mush containing mafic minerals was squeezed out to form the sulfide-poor lherzolite of the Jinchuan body. The giant sulfide ore bodies in the lower part of the Jinchuan body are attributed to injection of sulfide-bearing crystal-mush after emplacement of the lherzolite. Flow differentiation concentrated the sulfide in the central parts of the orebodies, such as in ore body 1.

Conclusions

The giant Jinchuan Ni-Cu-(PGE) sulfide ore bodies are hosted in a dike-like ultramafic intrusion. The high-Mg tholeiitic magmas experienced AFC processes, reached S-saturation, and formed a compositionally zoned magma body in a staging magma chamber at depth. The sulfide-poor, and crystal-free magmas from the upper portion in the staging magma chamber were squeezed out at an early stage. The sulfide-poor, crystal-mush, and sulfide-bearing crystal-mush were then squeezed out sequentially to form the Jinchuan body, with sulfide orebodies in the central and lower parts of the intrusion.

Acknowledgments

This study was supported by research grants (HKU7056/03P) from the Research Grant Council (RGC) of Hong Kong SAR (China) to M.-F. Zhou, and by the "CAS Hundred Talents" Project of the Chinese Academy of Sciences and NSFC grant (40573014) to X.-Y. Song. Reviews by W. G. Ernst and beneficial comments and suggestions of Paul T. Robinson and Jason R. Ali are gratefully appreciated. Many thanks to the Jinchuan mine personnel for their generous logistical support during the field work.

REFERENCES

Arndt, N. T., Czamanske, G. K., Walkerm, R. J., Chauvel, C., and Fedorenko, V. A., 2003, Geochemistry and origin of the intrusive hosts of the Noril'sk-Talnakh Cu-Ni-PGE sulfide deposits: Economic Geology, v. 98, p. 495–515.

Barnes, S. J., and Tang, Z. L., 1999, Chrome spinels from the Jinchuan Ni-Cu sulfide deposit, Gansu province, People's Republic of China: Economic Geology, v. 94, p. 343–356.

Brugmann, G. E., Naldrett, A. J., Asif, M., Lightfoot, P. C., Gorbachev, N. S., and Fedorenko, V. A., 1993, Siderophile and chalcophile metals as traces of the evolution of the Siberian Traps in the Noril'sk region, Russia: Geochimica et Cosmochimica Acta, v. 57, p. 2001–2018.

Chai, G., and Naldrett, A. J., 1992a, The Jinchuan ultramafic intrusion: Cumulate of a high-Mg basaltic magma: Journal of Petrology, v. 33, p. 277–303.

Chai, G., and Naldrett, A. J., 1992b, Characteristics of Ni-Cu-PGE mineralisation and genesis of the Jinchuan deposit, Northwest China: Economic Geology, v. 87, p. 1475–1495.

Carlson, R. W., 1991, Physical and chemical evidence on the cause and source characteristics of flood basalt volcanism: Australian Journal of Earth Sciences, v. 38, p. 525–544.

De Waal, S. A., and Xu, Z., 2004, Emplacement of viscous mushes in the Jinchuan ultramafic intrusion, western China: The Canadian Mineralogist, v. 42, p. 371–392.

Haughton, D. R., Roeder, P. L., and Skinner, B. J., 1974, Solubility of sulfur in mafic magma: Economic Geology, v. 69, p. 451–467.

Hawkesworth, C. J., Rogers, N. W., and Vancalsteren, P. W. C., 1984, Mantle enrichment processes: Nature, v. 311, p. 331–335.

Hawkesworth, C. J., Lightfoot, P. C., Fedorenko, V. A., Blake, S., Naldrett, A. J., Doherty, W., and Gorbachev, N. W., 1995, Magma differentiation and mineralization in the Siberian continental flood basalts: Lithos, v. 34, p. 61–88.

Hergt, J. M., Peate, D. W., and Hawkesworth, C. J., 1991, The petrogenesis of Mesozoic Gondwana low-Ti flood

basalts: Earth and Planetary Science Letters, v. 105, p. 398–416.

Hiemstra, S. A., 1986, The distribution of chalcophile and platinum-group elements in the UG-2 chromitite layer of the Bushveld Complex: Economic Geology, v. 81, p. 1080–1086.

Hofmann, A. W., 1988, Chemical differentiation of the Earth: the relationship between mantle, continental crust, and oceanic crust: Earth and Planetary Science Letters, v. 90, p. 297–314.

Irvine, T. N., 1975, Crystallization sequence of the Muskox Intrusion and other layered intrusions: II. Origin of the chromitite layers and similar deposits of other magmatic ores: Geochimica et Cosmochimica Acta, v. 39, p. 991–1020.

Keays, R. R., 1995, The role of komatiitic and picritic magmatism and S-saturation in the formation of the ore deposits: Lithos, v. 34, p. 1–18.

Li, C., Lightfoot, P. C., Amelin, Y., and Naldrett, A. J., 2000, Contrasting petrological and geochemical relationships in the Voisey's Bay and Mushuau intrusions, Labrador, Canada: Implications for ore genesis: Economic Geology, v. 95, p. 771–800.

Li, C., Maier, W. D., and De Waal, S. A. D., 2001, The role of magma mixing in the genesis of PGE mineralization in the Bushveld complex: Thermodynamic calculation and new interpretations: Economic Geology, v. 96, p. 653–662.

Li, C., Xu, Z., Sybrand, A., De Waal, S. A., Ripley, E. M., and Maier, W. D., 2004, Compositional variations of olivine from the Jinchuan Ni-Cu sulfide deposit, western China: Implication for ore genesis: The Canadian Mineralogist, v. 39, p. 159–172.

Li, X. H., Su, L., Chung, S.-L., Li, Z. X., and Liu, Y., 2005, Formation of the Jinchuan ultramafic intrusion and the world's third largest Ni-Cu sulfide deposit: Associated with the 825 Ma South China mantle plume?: Geochemistry, Geophysics, Geosystems, v. 6, pp. 16.

Lightfoot, P. C., Hawkesworth, C. J., Hergt, J., Naldrett, A. J., Gorbachev, N. S., Fedorenko, V. A., and Doherty, W., 1993, Remobilisation of the continental lithosphere by a mantle plume: Major-, trace-element, and Sr- Nd- and Pb-isotope evidence from picritic and tholeiitic lavas of the Noril'sk district, Siberian Traps, Russia: Contributions to Mineralogy and Petrology, v. 114, p. 171–188.

Lightfoot, P. C., and Naldrett, A. J., 1999, Geological and geochemical relationships in the Voisey's Bay intrusion, Nain plutonic suite, Labrador, Canada, *in* Keays, R. R., Lesher, C. M., Lightfoot, P. C., and Farrow, C. E. G., eds., Dynamic processes in magmatic ore deposits and their application in mineral exploration: Geological Association of Canada, Short Course Volume 13, p. 1–30.

Lightfoot, P. C., Naldrett, A. J., Gorbachev, N. S., Doherty, W., and Fedorenko, V. A., 1990, Geochemistry of the Siberian Trap of the Noril'sk area, USSR, with implication for the relative contribution of crust and mantle to flood basalt magmatism: Contributions to Mineralogy and Petrology, v. 104, p. 631–644.

Lightfoot, P. C., Naldrett, A. J., Gorbachev, N. S., Fedorenko, V. A., Hawkesworth, C. J., Doherty, W., 1994, Chemostratigraphy of Siberian flood basalts lavas, Noril'sk district, Russia: Implication and source of flood basalt magmas and their associated Ni-Cu mineralization, *in* Lightfoot, P. C., and Naldrett, A. J., eds., Proceedings of the Sudbury-Noril'sk symposium: Ontario Geological Survey Special Publication no. 5, p. 283–312.

Mahoney, J. J., 1988, Deccan Traps, *in* Macdougall, J. D., Continental flood basalts: Dordrecht, The Netherlands, Kluwer Academic Publishers.

Naldrett, A. J., 1989, Magmatic sulfide deposits: New York, NY, Oxford University Press.

Naldrett, A. J., 1999, World-class Ni-Cu-PGE deposits: Key factors in their genesis: Mineralium Deposita, v. 34, p. 227–240.

Naldrett, A. J., Fedorenko, V. A., Lightfoot, P. C., Gorbachev, N. S., Doherty, W., Asif, M., Lin, S., and Johan, Z., 1995, A model for the formation of the Ni-Cu-PGE deposits of the Noril'sk: Transactions of the Institution of Mining and Metallurgy, v. 104, B18–B36.

Naldrett, A. J., and Lightfoot, P. C., 1999, Ni-Cu-PGE deposits of the Noril'sk region, Siberia: Their formation in conduits for flood basalt volcanism, *in* Keays, R. R., Lesher, C. M., Lightfoot, P. C., and Farrow, C. E. G., eds., Dynamic processes in magmatic ore deposits and their application in mineral exploration: Geological Association of Canada, Short Course Volume 13, p. 195–249.

Naldrett, A. J., Lightfoot, P. C., Fedorenko, V. A., Gorbachev, N. S., and Doherty, W., 1992, Geology and geochemistry of intrusions and flood basalts of the Noril'sk region, USSR, with implication for the origin of the Ni-Cu-PGE ores: Economic Geology, v. 87, p. 975–1004.

Peach, C. L., Mathez, E. A., and Keays, R. R., 1990, Sulfide melt-silicate melt distribution coefficients for noble metals and other chalcophile elements as deduced from MORB: Implication for partial melting: Geochimica et Cosmochimica Acta, v. 54, p. 3379–3389.

Qi, L., Hu, J., and Gregoire, D. C., 2000, Determination of trace elements in granites by inductively coupled plasma mass spectrometry: Talanta, v. 51, p. 507–513.

Qi, L., Zhou, M.-F., and Wang, C. Y., 2004, Determination of low concentrations of platinum group elements in geological samples by ID-ICP-MS: Journal of Analytical Atomic Spectrometry, v. 19, p. 1335–1339.

Song, X.-Y., 2004, Geochemistry of Permian flood basalts and related Ni-Cu-(PGE) sulfide-bearing sills in Yangliuping, Sichuan Province, China: Unpubl. Ph.D thesis, University of Hong Kong.

Song, X.-Y., Zhou, M.-F., Cao, Z.-M., Sun, M., and Wang, Y.-L., 2003, The Ni-Cu-(PGE) magmatic sulfide deposits in the Yangliuping area within the Permian Emeishan Large Igneous Province, SW China: Mineralium Deposita, v. 38, p. 831–843.

Tang, Z. L., 1991, Formation of the Jinchuan Cu-Ni sulfide deposit: Modern Geology, v. 4, p. 55–64 (in Chinese).

Tang, Z. L., and Barnes, S. J., 1998, Mineralization mechanism of magmatic sulphide deposits: Beijing, China, Geological Publishing House.

Tang, Z. L., and Li, W. Y., 1995, Mineralisation model and geology of the Jinchuan Ni-Cu sulfide deposit bearing PGE: Beijing, China, Geological Publishing House.

Tang, Z. L., Yang, J. D., Xu, S. J., Tao, X. C., and Li, W. Y., 1992, Sm-Nd dating of the Jinchuan ultramafic rock body, Gansu, China: Chinese Science Bulletin, v. 37, p. 1988–1990.

Taylor, S. R., and McLennan, S. M., 1985, The continental crust: its composition and evolution: Oxford, UK, Blackwell.

Von Gruenewaldt, G., Hatton, C. J., and Naldrett, A. J., 1986, Contrasting platinum-group element-chromitite associations in cumulates of the Bushveld Complex: Economic Geology, v. 81, p. 1067–1079.

Wooden, J. L., Czamanske, G. K., Fedorenko, V. A., Arndt, N. T., Chauvel, C., Bouse, R. M., King, B-S. W., Knight, R. J., and Siems, D. F., 1993, Isotopic and trace-element constrains on mantle and crustal contributions to Siberian continental flood basalts, Noril'sk area, Siberia: Geochimica et Cosmochimica Acta, v. 57, p. 3677–3704.

Yang, X.-Z., Ishihara, S., and Matsueda, H., 1998, Multiphase melt inclusions in the Jinchuan complex, China: Implications for petrogenetic and metallogenic physico-chemical condition: International Geology Review, v. 40, p. 335–349.

Zhao, G. C., Sun, M., Wilde, S. A., and Li, S. Z., 2005, Late Archean to Paleoproterozic evolution of North China: Key issues revisited: Precambrian Research, v. 136, p. 177–202.

Zhou, M.-F., Malpas, J., Song, X., Robinson, P. T., Sun, M., Kennedy, A. K., Lesher, M., and Keays, R. R., 2002a, A temporal link between the Emeishan Large Igneous Province (SW China) and the end-Guadalupian mass extinction: Earth and Planetary Science Letters, v. 196, p. 113–122.

Zhou, M.-F., Yang, Z.-X., Song, X.-Y., Keays, R. R., and Lesher, C. M., 2002b, Magmatic Ni-Cu-(PGE) sulfide deposits in China, *in* Cabri, L. J., ed., The geology, geochemistry, mineralogy, and mineral beneficiation of the platinum-group elements: Canadian Institute of Mining, Metallurgy, and Petroleum, Special Volume 54, p. 619–636.